Published in final edited form as:
Proteomics. 2013 October ; 13(20): . doi:10.1002/pmic.201300142.

Characterization of Multiple Myeloma Vesicles by Label-Free Relative Quantitation

Sean W. Harshman[1,2,¥], **Alessandro Canella**[2,¥], **Paul D. Ciarlariello**[2], **Alberto Rocci**[7], **Kitty Agarwal**[4,6], **Emily M. Smith**[2], **Tiffany Talabere**[2], **Yvonne A. Efebera**[3], **Craig C. Hofmeister**[3], **Don M. Benson Jr.**[3], **Michael E. Paulaitis**[5,6], **Michael A. Freitas**[1,2,*], and **Flavia Pichiorri**[3,*]

[1]Department of Molecular Virology, Immunology and Medical Genetics, The Ohio State University, Columbus, OH, USA

[2]Comprehensive Cancer Center, The Ohio State University, Columbus, OH, USA

[3]Department of Internal Medicine, Division of Hematology, The Ohio State University, Columbus, OH, USA

[4]Department of Chemistry and Biochemistry, The Ohio State University, Columbus, OH, USA

[5]Department of Chemical and Biomolecular Engineering, The Ohio State University, Columbus, OH, USA

[6]Nanoscale Science and Engineering Center, The Ohio State University, Columbus, OH, USA

[7]Myeloma Unit, Division of Hematology, University of Turin, Azienda Ospedaliera Cittá della Salute e della Scienza di Torino, 10126 Torino, Italy

Abstract

Multiple myeloma (MM) is a hematological malignancy caused by a microenviromentally aided persistence of plasma cells in the bone marrow. The role that extracellular vesicles, microvesicles and exosomes, released by MM cells have in cell-to-cell communication and signaling in the bone marrow is currently unknown. This paper describes the proteomic content of extracellular vesicles derived from MM.1S and U266 MM cell lines. First, we compared the protein identifications between the vesicles and cellular lysates of each cell line finding a large overlap in protein identifications. Next, we applied label-free spectral count quantitation to determine proteins with differential abundance between the groups. Finally, we used bioinformatics to categorize proteins with significantly different abundances into functional groups. The results illustrate the first use of label-free spectral counting applied to determine relative protein abundances in extracellular vesicles.

Keywords

Extracellular vesicles; Microvesicles; Exosomes; Proteomics; Label-Free; LC-MS/MS

[*]Address reprint requests to: Dr. Michael A. Freitas, The Ohio State University Medical Center, 460 West 12th Avenue, Columbus, OH 43210, USA. Phone (614) 688-8432, Fax (614) 688-8675, freitas.5@osu.edu or Dr. Flavia Pichiorri The Ohio State University Medical Center, 460 West 12th Avenue, Columbus, OH 43210, USA. Phone 614-688-8071 Fax (614) 688-8675, flavia.pichiorri@osumc.edu.
[¥]These authors contributed equally to this work.

INTRODUCTION

Multiple myeloma (MM) is the second most common hematological malignancy accounting for more than 10,000 deaths annually [1]. Recent improvements in antineoplastic drugs including proteasome inhibitors and immune modulating drugs (IMiD's) have improved overall patient outcomes [2]. There is a tight relationship between MM plasma cells (PC's) and the bone marrow (BM) stromal cells (BMSC's), and this stroma has a pivotal role in the regulation of MM cell growth and survival, as well as soluble factors and adhesion molecules [3]. Although important soluble factors and adhesion molecules, such as TNF-α and CD49d have been identified, small lipid-membrane bound vesicles are hypothesized to also play a role in cell-cell signaling [3–5]. Microvesicles or exosomes (called extracellular vesicles or EV), released by almost all cell types, are small structures based on a lipid bilayer and are recognized as important in facilitating intercellular communication without cell-to-cell contact. Recently, several studies have focused on the role of circulating extracellular vesicles in cancer biology. These vesicles increase tumor survival and expansion by carrying bioactive mRNA, miRNA and proteins into the extracellular space allowing for functional manipulation of the surrounding tumor microenvironment [4,5].

Mass Spectrometry based proteomics is a powerful tool used to characterize the protein content of extracellular vesicles [6–31]. In this manuscript we used shotgun proteomics to identify proteins contained in vesicles derived from two distinct MM cell lines. We further applied label-free spectral count relative quantitation to assess the differences in protein abundances [32,33]. This approach revealed proteins of variable abundance across these MM cell-derived vesicles. Our results establish a foundation for further functional studies of MM biology through the identification of proteins associated with vesicle targets.

EXPERIMENTAL

Cell Line Tissue Culture

MM.1S and U266 cell lines were obtained from American Type Culture Collection (ATCC, Manassas, VA, USA) and cultured using modified conditions originally described by Goldman-Leikin et al. and Nilsson et al. [34,35]. Briefly, cells were maintained at 0.4×10^6 cells/ml by incubation at 37 °C with 5 % CO_2 in RPMI-1640 media supplemented with 10 % fetal bovine serum (FBS), 2 mM glutamine (GlutaMAX), 50 U/mL penicillin-G and 50 μg/mL streptomycin (Life Technologies, Grand Island, NY). To eliminate artifacts from serum-derived vesicles, 48 hours before analysis, $100–200 \times 10^6$ cells were pelleted at 300 × g for 10 min and resuspended in serum free media at $1–1.5 \times 10^6$ cells/ml.

Vesicle Isolation

The method used for isolation of cell line derived vesicles was previously described by Théry et al. [36]. In short, serum starved cells and media were centrifuged at 300 × g for 10 min at 4 °C. Supernatant was collected and centrifuged again at 2000 × g for 20 min at 4 °C. The cell pellets were frozen and stored at −80 °C for later use. Supernatant was harvested and vacuum ultracentrifuged at 10,000 × g for 30 min at 4 °C to remove residual cell debris. Supernatant was collected and ultracentrifuged at 100,000 × g for 70 min at 4 °C with vacuum. The resulting supernatant was discarded, pellets from multiple tubes were resuspended in 1 ml of PBS, pooled into a single tube, and ultracentrifuged at 100,000 × g as described previously. Supernatant was eliminated and pellets of vesicles were frozen and stored at −80 °C.

Flow Cytometry

MM.1S and U266 cell lines were analyzed for Annexin V and propidium iodide staining. Following serum starvation, cells were washed 1x with PBS and Annexin V and Propidium Iodide staining solution (Clonetech Laboratories, Mountain View, CA) was added. Samples were allowed to stand for 15 min in the dark. Cells were washed 1x with PBS and immediately analyzed. All analyses were completed on a Beckman Coulter CXP flow cytometer (Beckman Coulter, Brea, CA).

Cryo-Transmission Electron Microscopy (cryo-TEM)

Vesicles derived from MM1. S and U266 cells were prepared for cryo-TEM within a controlled environment (22°C and 95% relative humidity) of an automated vitrification device (FEI Vitrobot Mark IV, FEI, Hillsboro, OR). To prepare vitrified specimens, 4 μl suspensions of extracellular vesicles were applied to glow discharged lacey carbon coated copper grids (400 mesh, Pacific Grid-Tech, San Francisco, CA) and flash-frozen in liquid ethane. The vitrified samples were stored under liquid nitrogen before transferring to a Gatan Cryo holder (Model 626.DH) and visualized in a FEI Tecnai G2 F20 ST transmission electron microscope (TEM, FEI, Hillsboro, OR). The microscope was operated at 200kV and under low dose mode to minimize radiation damage to the samples. Images were captured using a 4k × 4k Gatan Ultrascan CCD camera at a magnification of 38,000×.

Dynamic Light Scattering (DLS)

Number distributions of extracellular vesicle hydrodynamic diameters were derived from DLS measurements using a Nano Zetasizer Zen3600 (Malvern Instruments Ltd., Worcestershire, United Kingdom). Samples were diluted to the required count rate of 50–300 kilocounts per second and equilibrated at 25°C. All measurements were made in triplicate. The Stokes-Einstein relation was used to calculate particle diameters from measured translational diffusion coefficients.

Preparation of Samples for Mass Spectrometry

The preparation of both the cell-derived vesicles and the global lysates was done following a modified method previously developed in our lab [32]. Briefly, triplicates of vesicle isolations or 48 h serum starved cell pellets (100,000 cells) were resuspended in 50 mM ammonium bicarbonate (Sigma Aldrich, St. Louis, MO) supplemented with 0.5 % Rapigest SF surfactant (Waters, Milford, MA). 800 ng of sequencing grade modified trypsin (Promega, Madison, WI) was added to each sample and incubated overnight (>16h) at 37 °C. The reaction was suspended and Rapigest was precipitated through the addition of 98% formic acid (Acros Organics, Geel, Belguim) to approximately 30 % v/v. Samples were returned to 37 °C for 30 min. Solutions were centrifuged 3x at 21,000 × g removing the supernatant following each centrifugation. Peptides were speedvac'd to dryness and resuspended in 20 μl of 2 % acetonitrile with 0.1 % formic acid (aq). Final peptide concentrations were measured by 280 nm absorbance using a NanoDrop ND-1000 (NanoDrop, Wilmington, DE) spectrometer.

Liquid Chromatography Mass Spectrometry (LC-MS/MS)

1–2 μg of peptides were loaded for RP-HPLC separation on a Dionex Ultimate 3000 capillary/nano HPLC (Dionex, Sunnyvale, CA) and mass analyzed by a ThermoFisher LTQ Orbitrap XL mass spectrometer (ThermoFisher, Waltham, MA). The LTQ Orbitrap XL was fitted with a micro/nanospray ionization source (Michrom Bioresources Inc, Auburn, CA). HPLC separations were carried at a flow rate of 2 μl/min on a 0.2 mm × 150 mm C18 column (5 μm, 300 Å, Michrom Bioresources Inc., Auburn, CA). Mobile phases were HPLC water (J.T. Baker, Center Valley, PA) and acetonitrile (EMD Millipore, Billerica, MA) each

supplemented with 0.1 % (v/v) formic acid. The 300 minute HPLC gradient was as follows. Starting at 2 % mobile phase B the gradient was increased linearly to 5 % at 12 min, 15 % at 40 min, 30 % at 170 min, 55 % at 240 min, 85 % at 265 min and 90% at 270 min. The column was held at 90 % for five minutes, followed by equilibration at 2 % for 24 min. The heated capillary temperature and electrospray voltage on the LTQ Orbitrap XL were 175 °C and 2.0 kV, respectively. Top 5 data dependent mode was utilized in positive ion mode with dynamic exclusion of: repeat count=3, repeat duration=30.00, exclusion list size=500, exclusion duration=350 s and exclusion mass width of ± 1.50 m/z. Protein identifications were obtained using the MassMatrix search engine (v 2.4.2) and the UniprotKB complete H. sapiens proteome (as of 18Sep12) [37–40]. Search parameters included three trypsin missed cleavages, precursor ion tolerance of ± 10 ppm and a product ion tolerance of ± 0.8 ppm. Cytoskeletal, epidermal and cuticle keratin identifications were recognized as contaminant proteins and removed from the analysis (listed in Supplemental Data 4–8). The false discovery rate (FDR) was estimated using the reversed sequences of the target database. The parsing of protein identifications and spectral counts was conducted from each data file and combined using an in-house python application [41]. For combined protein lists, the protein matches were retained based on an FDR threshold of 5 % and 2 unique peptide matches or a max decoy cutoff of 2 for each set of protein identifications.

Label-Free Relative Quantitation

Relative quantitation of the LC-MS/MS data was performed using the label-free approach described by Liu et al. and Colinge et al. [42,43]. The spectral counts used in the analysis did not include modified, semi-tryptic or shared peptides, including those from multiple protein isoforms. Protein lists were generated as follows. Search results were combined into a single harmonized table. This table contains the protein ID, the number of spectral counts, the number of peptides, sequence coverage and protein scores. Proteins were grouped based on common peptide sets. Each protein group is represented by the protein ID with the highest number of spectral counts. Spectral count quantitation was performed using only the the top protein matches that had tow or more distinct peptide sequences in at least one sample and protein scores above the decoy match discriminant score threshold. The decoy match discrimanty score was determined by taking the the protein score for the third decoy match or the decoy score that exceeds the target-decoy false dicovery rate of 5%. Spectral count quantitation was performed on the proteins that had a minimum of 5 total spectral counts across all samples. These criteria are very conservative and may reduce the apparent limit of detection because rare protein matches with low counts are removed from the quantitative analysis. The spectral count data and their estimated FDRs are provided in Supplemental Data 5–8. Significance analysis of relative protein abundance from spectral count data was determined by using the edgeR bioconductor package [44]. Peptide spectral count distributions were modeled using a Poisson/negative binominal distribution and normalized to the respective spectral count library size [44–46]. Differences in protein abundance were evaluated based upon an exact text for the overdispersed data [46]. False discovery was controlled by applying a Benjamini-Hochberg multi-test correlation (α = 0.05) to final p-values [47]. Counts per million (CPM) were calculated as the base 2 log of the normalized average counts across a row divided by one million.

Computational Annotations, Clustering and Bioinformatics

Venn diagrams were created using the BioVenn web application (http://www.cmbi.ru.nl/cdd/biovenn/) [48]. Clustering analysis and visualization was performed using open source software Cluster 3.0 and Java Tree View (ver. 1.1.6r2). Bioinformatic annotations of gene ontology for identified proteins were searched against the PANTHER Classification System (http://www.pantherdb.org/) [49,50].

Immunoblotting

Cell and vesicles were lysed using a modified RIPA buffer (50 mM Tris pH 7.5, 150 mM NaCl, 10 % Glycerol, 1.0% % NP-40, 0.1% SDS and protease and phosphatase inhibitors). Protein concentrations of the lysates were determined by Bradford assay (Bio-Rad, Richmond, CA). Equivalent amounts of global lysates and vesicle lysates were run in a 4–15 % Tris-HCl SDS-PAGE TGX gel (Bio-Rad, Richmond, CA), transferred to nitrocellulose and blotted for CD9, CD44, Actin and Nucleolin (NCL, Santa Cruz Biotechnology, Santa Cruz, CA), glyceraldehyde 3-phosphate dehydrogenase (GAPDH, Cell Signaling Technology, Boston, MA), and IgG Kappa Light Chain, Major Histocompatibility Complex Class I, and Bone Marrow Stromal Cell Antigen 2 (IgGκ LC, MHC Class I, BST-2, Abcam, Cambridge, MA). Chemiluminescent detection was performed using anti-mouse & anti-rabbit IgG-HRP (GE Healthcare, Piscataway, NJ) and either ECL Western Blotting Detection Reagents (GE Healthcare, Piscataway, NJ) or SuperSignal West Femto Kit (Pierce Biotechnology, Rockford, IL). HeLa (CD9) and ARH77 (IgGκ LC) global lysates were used as positive controls for the immunoblots.

RESULTS

Size Distribution and Structural Characteristics of MM derived Vesicles

The MM cell-derived vesicles were imaged by cryo-TEM to obtain morphological characteristics. Figures 1A & 1B show representative cryo-TEM images of vesicles derived from the MM.1S and U266 cell lines. The images depict vesicles that are spherical in shape with a single lipid bilayer, and hydrodynamic diameters that range from roughly 50 to 200 nm. Several vesicles are observed to contain daughter vesicles (Figure 1A, **Top**) or internal, electron dense material (Figure 1B, **Top**). Dynamic light scattering (DLS) was performed to assess the size distributions of the enriched vesicles. The DLS analysis of the U266 derived vesicles shows a monomodal distribution of vesicle diameters ranging from 80–200 nm (average diameter of 138 nm), while the MM.1S vesicle diameters are somewhat larger, ranging from 100–200 nm (average diameter of 177 nm) with a small population of even larger vesicles with diameters between 240 and 260 nm (Figure 1C). Collectively, these results indicate that our MM cell-derived vesicle preparations yield extracellular vesicles with similar size distributions and similar spherical morphologies for the two cell lines [4].

It has been shown that apoptotic cells release organelle-containing vesicles as part of their death program [51]. It is possible therefore that vesicle isolations may contain apoptotic bodies. To address the possibility of apoptotic body contamination in our vesicle preparations, Annexin V/popidium iodide flow cytometry was conducted on serum starved cells prior to vesicle isolation. Supplemental Data 1 shows greater than 98 % of cells are negative for Annexin V/popidium iodide staining. Confirming that the majority of the vesicles are derived from cells that are non-apoptotic. Taken together, the data indicate that vesicles obtained from nonapoptotic MM.1S and U266 MM cell lines have diameters between 0–200 nm.

Proteomics of MM Cell Line Derived Vesicles

Vesicles isolated from the MM.1S and U266 cell lines and the corresponding global cell lysates were characterized by liquid chromatography tandem mass spectrometry (LC-MS/MS) proteomic analysis. An overview of the proteomic workflow used is provided in Supplemental Data 2. The LC-MS/MS base peak chromatograms for the vesicles and cell lysates (Supplemental Data 3 & 4) show high similarity. A database search of the LC-MS/MS from three experimental replicates (starting from cells grown from separate cultures) for each of the vesicles yielded 311 and 272 protein identifications for the MM.1S and U266 cell lines, respectively (Supplemental Data 5 & 6). The LC-MS/MS analysis of the global

MM.1S and U266 cell lysates yielded 279 and 353 protein identifications (Supplemental Data 7 & 8). Venn diagrams are provided in Figures 2A & 2B to show the overlap in protein identifications between the cell-derived vesicles and their global lysates. While there is a high number of overlapping protein IDs, unique proteins were observed in the cell line derived vesicles (24%, 72 for MM.1S and 15%, 49 for U266) and the lysates (18%, 55 for MM.1S and 35%, 111 for U266).

Recent literature on protein composition of vesicles obtained from many cell lines reported that several proteins are similar irrespective of cell of origin [52–54]. However, vesicles may also harbor proteins unique to the cell of origin. To determine if this hypothesis holds true for our data set, we compared the protein IDs in MM.1S and U266 vesicles. The Venn diagram in Figure 2C shows 32 (10%) proteins unique to the MM.1S vesicles and 13 (4%) proteins unique to U266 with 324 common proteins. Additionally, comparison of the MM. 1S and U266 vesicle identifications to the downloadable ExoCarta database of EV identified proteins yield a large number of previously identified proteins (83% MM.1S and 77% U266, Supplemental Data 5 & 6) [30,31]. These results are consistent with recent proteomic analyses of extracellular vesicles [30,31,53,54].

Label-Free Comparison of Cellular Proteins and Vesicles

The LC-MS/MS data show a high similarity in protein IDs between the cell-derived vesicles and their corresponding cellular lysates. Hierarchical cluster analysis reveals significant differences in the relative protein spectral counts between vesicle and cellular proteins. Cluster heat maps are provided along with ontological classification of the protein molecular functions and biological processes (Figure 3). Label-free spectral count quantitation was then used to determine the significance of relative differences in protein abundance [32,33]. Relative quantitation determined 298 and 366 proteins with significant differences in protein spectral counts between the MM.1S and U266 vesicles and their corresponding cellular lysates ($p < 0.05$) (Supplemental Data 9). Classification of significant proteins by molecular functions and biological processes determined, using the PANTHER gene ontological search software, that vesicles have significantly different protein abundance than their cell of origin (Figure 3).

Hierarchical clustering of the MM.1S and U266 vesicles shows tight grouping by cell of origin (Figure 4A). Label-free relative quantitation determined 125 proteins with significantly different abundance between the MM.1S and U266 vesicles ($p < 0.05$) (Table 1 & Supplemental Data 9). The smear plot (constructed by plotting the log fold change (logFC) vs log counts-per-million (logCPM)) is provided in Figure 4C. The PANTHER gene ontological annotations for biological process and molecular function for those proteins with statistically different abundance are provided in Figure 4D. These data suggest the protein abundances in vesicles can distinguish between the cells of origin. Additionally, the results show that the measurement of these differences in relative abundance more closely reflects biologic function than protein ID alone.

The increase in the relative abundance of specific proteins in the vesicles could be attributed to higher protein expression in a given cell type rather than specific packaging of proteins into the vesicles. To determine if the differences in vesicular protein compositions are driven by cell type vs. packaging, we plotted the fold change (Log FC) of each protein in the MM. 1S vs. U266 vesicles vs. its corresponding change in the cellular protein. Figure 5A shows proteins with no significant change in vesicular abundance or cellular expression in the same direction (i.e. both increased/decreased in the vesicles and global lysates). As expected these data points cluster about a line with a slope of 1 indicating vesicle abundance was driven predominantly by expression in the parent cell type. Conversely, Figure 5B highlights the proteins with opposing significant differences between the vesicles and cellular lysates (i.e.

increased abundance or expression in one sample type while the other remains unchanged or decreases). These data primarily cluster about the 0 intercept. However, there are several proteins located in the upper left and lower right quadrant that are significantly enriched in the vesicle samples independent of changes in the cellular protein abundance (Figure 5C). For the complete list of proteins with independent changes in abundance see Supplemental Data 10. These results illustrate the power of the label free approach in establishing the patterns of abundance of vesicular proteins relative to cellular expression revealed in the global lysate expression.

Validation of LC-MS/MS Protein Identifications and Relative Quantitation

To validate proteomic identifications and relative quantitation, we conducted immunoblots on the cell-derived vesicles (Figure 6A) and both vesicles and parent cell lysates (Figure 6B). Based on the LC-MS/MS data (Table 1 & Supplemental Data 9) and antibody availability, several proteins were identified for validation by immunoblot. First, CD9 was selected, as it was not identified in the U266 derived vesicles while showing enrichment in the MM.1S released vesicles. Conversely, IgG kappa light chain (IgGκ LC) was selected due to LC-MS/MS identification in U266 derived vesicles while remaining undetected in the MM.1S vesicles. Next, Nucleolin was identified for validation because the MS data showed enrichment in the MM.1S vesicles compared to the U266 vesicles. Finally, glyceraldehyde 3-phosphate dehydrogenase (GAPDH) was chosen as it was identified in both the MM.1S and U266 derived vesicles. The immunoblot shown in Figure 6A confirms the presence and relative abundances of CD9, IgGκ LC, Nucleolin and GAPDH in the vesicles derived from the respective cell lines as described above.

Further validation of the LC-MS/MS derived relative abundances was confirmed through a second immunoblot containing both vesicle and cell lysates (Figure 6B). First as above, CD9 was shown by mass spectrometry to be only identified in the vesicles of the MM.1S cell line. The blot in Figure 6B further confirms the MS data and Figure 6A for the identification of CD9. Additionally, the LC-MS/MS data shows CD44, MHC Class I and BST-2 were enriched in the vesicles of both cell lines when compared to the cell lysates. The immunoblot shown in Figure 6B confirms the mass spectrometry data shown in Table 1 and Supplemental Data 9 for CD9, CD44, MHC Class I and BST-2 proteins. Both GAPDH and Actin were blotted as housekeeping genes. However due to challenges in protein loading associated with vesicles, the common housekeeping genes are not completely adequate for normalization proposes in this sub-cellular fraction. Regardless, the immunoblots confirm the relative changes we observe in the proteomics experiments while also exposing challenges in normalization of protein abundances between vesicles and cells.

DISCUSSION

Cellular communication through soluble factors and cell-to-cell adhesion molecules has long been established for many hematological cell types including MM [55]. Until recently, the role of vesicular communication between cells has gone relatively unstudied. Limitations in sample management, purity and preparation yield make vesicle study challenging. The monomodal size distributions of the vesicles isolated from both MM cell lines suggest a single, monodisperse population of vesicles in each case. The MM.1S vesicles are somewhat larger (average diameter of 177 nm) and have a slightly broader size distribution (standard deviation of 6.2 nm) compared to the U266 vesicles: average diameter of 138 nm and a standard deviation of 5.6 nm. These average diameters and size distributions correspond approximately to the exosome sub-population of cell-secreted vesicles [4]. The similarity of the proteomic identifications between the vesicle populations also suggests similar vesicle populations for the two MM cell lines.

Proteomic analysis of cell-derived vesicles has become the primary tool for vesicular protein characterization. Mainly in the last decade, vesicles from many *in vitro* and *in vivo* origins have been analyzed by various MS methods [6–31]. Our study represents an advance in vesicular proteomics through the use of label-free relative quantitation to characterize MM cell-derived vesicles and global lysates. We identified 583 total vesicular proteins from the MM.1S and U266 vesicles. Although the LC-MS/MS data identified a number of common extracellular vesicle proteins, such as antigen presenting molecules (MHC class I and class II), adhesion molecules (tetraspanins and integrins), membrane transport and fusion molecules (annexins, flotillin and Rab proteins), cytoskeletal proteins (actin, tubulin and moesin), and many others such as pyruvate kinase, GAPDH, 14-3-3 proteins, HSP70, HSP90, elongation factor 1α and the histones H2B, H2A, and H4, we also identified 32 and 13 proteins unique to the vesicles derived from the MM.1S and U266 cell lines, respectively [52–54]. These results support the hypothesis that extracellular vesicles have common protein profiles in large part, but with small sets of unique proteins corresponding to the parent cells of origin [52–54]. Furthermore the exclusive presence of BST-2 in the EV compartment of MM cells strongly supports the specificity of our analysis.

While there are only a small number of different identifications between the MM.1S and U266 vesicles, the relative abundances of proteins in the MM cell-derived vesicles are more divergent. The label-free relative quantitation of the MM.1S and vesicle data sets shows 125 proteins with statistically different protein abundance. These proteins correspond to an array of functions both biologically and molecularly. For example, the RNA-binding protein Nucleolin (NCL) was shown to have higher abundance in the MM.1S vesicles. NCL is a highly conserved multifunctional protein, abundantly expressed in the nucleolus of normal cells [56]. It has long been known as a protein critical for ribosomal RNA biogenesis (rRNA) [56]. In the cytoplasm, NCL functions to regulate mRNA translation and stability of several tumor progression genes, including BCL2, thereby inhibiting apoptosis of cancer cells. NCL is an integral component of the DROSHA-DGCR8 microprocessor complex and recently we have shown that NCL promotes the maturation of a specific set of miRNAs that are implicated in the pathogenesis of several human cancers, such as miR-*21*, miR-*103*, miR-*221* and miR-*222*, whose over-expression is often associated with greater aggressiveness and resistance to anti-neoplastic therapies [57–60]. The presence of NCL and other RNA binding proteins in MM extracellular vesicles may allow further studies that will focus on the understanding their role in RNA transfer in cancer cells.

Alignment of vesicular and global cell lysate protein identifications shows a low number of unique identifications between the samples. Similar to the vesicle-to-vesicle comparisons, more divergent protein abundance was found with the application of the label-free edgeR analysis to the data sets. These data show 298 (MM.1S) and 268 (U266) proteins with variable abundance. For example, MM.1S vesicles show an increased abundance of HLA class II histocompatibility antigens when compared to the MM.1S global cell lysate. These results are in line with previous studies of B-cell derived exosomes [61,62]. Raposo et al. showed the vesicular MHC class II complexes can stimulate T-cells *in vitro* [61]. MHC class I has been identified as classical vesicle marker in the serum of cancer patients. The mechanisms of tumor cell resistance to immune effector functions are diverse and can be both intrinsic and reactive. A central immune escape route is the partial or complete down-regulation of this complex at the cell surface, thereby limiting or avoiding recognition by cytotoxic CD8+ T effector cells (CTLs) and the induction of apoptosis [63,64]. Based on these observations it is reasonable to hypothesize that the specific shedding of MHC class I can be a common characteristic of MM cells to avoid the immune system response and support their growth, although further studies in MM patients will be required to support this observation.

Finally, we are the first to apply a label-free approach to identify variably abundance among proteins in the vesicles and their parent cell. Our study reveals that only a small number of unique proteins are packaged into extracellular vesicles [52–54]. Our study also reveals a more divergent protein abundance in the vesicles of MM cell lines.

Supplementary Material

Refer to Web version on PubMed Central for supplementary material.

Acknowledgments

This work was supported by the Ohio State University, Pelotonia Fellowship Program (A.R.) and in part by grants from the NIH (R01 CA107106, P01 CA124570 and RC2 AG036559) and NSF (EEC-0425626 and EEC-019790).

The cryo-TEM data were obtained at the TEM facility at the Liquid Crystal Institute, Kent State University, supported by the Ohio Research Scholars Program Research Cluster on Surfaces in Advanced Materials. The authors thank Dr. Min Gao for technical support provided for the TEM experiments.

References

1. American Cancer Society. Cancer Facts & Figures. 2011. p. 1-68.
2. Kumar SK, Rajkumar SV, Dispenzieri A, Lacy MQ, et al. Improved survival in multiple myeloma and the impact of novel therapies. Blood. 2008; 111:2516–2520. [PubMed: 17975015]
3. Raje, N.; Hideshima, T.; Anderson, K.; Raphael, E.; Pollock, MD. Cancer medicine 8. Hong, WK.; Hait, WN.; Donald, W.; Kufe, MD.; Raphael, E.; Pollock, MD., editors. Pmph-usa; 2010. p. 2021
4. Théry C, Zitvogel L, Amigorena S. Exosomes: composition, biogenesis and function. Nat Rev Immunol. 2002; 2:569–579. [PubMed: 12154376]
5. Théry C. Exosomes: secreted vesicles and intercellular communications. F1000. Biol Rep. 2011; 3:15.
6. Bard MP. Proteomic Analysis of Exosomes Isolated from Human Malignant Pleural Effusions. American Journal of Respiratory Cell and Molecular Biology. 2004; 31:114–121. [PubMed: 14975938]
7. Miguet L, Pacaud K, Felden C, Hugel B, et al. Proteomic analysis of malignant lymphocyte membrane microparticles using double ionization coverage optimization. Proteomics. 2006; 6:153–171. [PubMed: 16342139]
8. Gonzales PA, Pisitkun T, Hoffert JD, Tchapyjnikov D, et al. Large-Scale Proteomics and Phosphoproteomics of Urinary Exosomes. Journal of the American Society of Nephrology. 2009; 20:363–379. [PubMed: 19056867]
9. Kesimer M, Scull M, Brighton B, DeMaria G, et al. Characterization of exosome-like vesicles released from human tracheobronchial ciliated epithelium: a possible role in innate defense. FASEB J. 2009; 23:1858–1868. [PubMed: 19190083]
10. Li Y, Zhang Y, Qiu F, Qiu Z. Proteomic identification of exosomal LRG1: A potential urinary biomarker for detecting NSCLC. ELECTROPHORESIS. 2011; 32:1976–1983. [PubMed: 21557262]
11. Staubach S, Razawi H, Hanisch FG. Proteomics of MUC1-containing lipid rafts from plasma membranes and exosomes of human breast carcinoma cells MCF-7. Proteomics. 2009; 9:2820–2835. [PubMed: 19415654]
12. Zhang Y, Li Y, Qiu F, Qiu Z. Comprehensive analysis of low-abundance proteins in human urinary exosomes using peptide ligand library technology, peptide OFFGEL fractionation and nanoHPLC-chip-MS/MS. ELECTROPHORESIS. 2010; 31:3797–3807. [PubMed: 21082674]
13. Mears R, Craven RA, Hanrahan S, Totty N, et al. Proteomic analysis of melanoma-derived exosomes by two-dimensional polyacrylamide gel electrophoresis and mass spectrometry. Proteomics. 2004; 4:4019–4031. [PubMed: 15478216]

14. Buschow SI, van Balkom BWM, Aalberts M, Heck AJR, et al. MHC class II-associated proteins in B-cell exosomes and potential functional implications for exosome biogenesis. Immunol Cell Biol. 2010; 88:851–856. [PubMed: 20458337]
15. Admyre C, Johansson SM, Qazi KR, Filén JJ, et al. Exosomes with immune modulatory features are present in human breast milk. J Immunol. 2007; 179:1969–1978. [PubMed: 17641064]
16. Wubbolts R. Proteomic and Biochemical Analyses of Human B Cell-derived Exosomes. POTENTIAL IMPLICATIONS FOR THEIR FUNCTION AND MULTIVESICULAR BODY FORMATION. Journal of Biological Chemistry. 2003; 278:10963–10972. [PubMed: 12519789]
17. Mathivanan S, Lim JWE, Tauro BJ, Ji H, et al. Proteomics analysis of A33 immunoaffinity-purified exosomes released from the human colon tumor cell line LIM1215 reveals a tissue-specific protein signature. Mol Cell Proteomics. 2010; 9:197–208. [PubMed: 19837982]
18. Welton JL, Khanna S, Giles PJ, Brennan P, et al. Proteomics analysis of bladder cancer exosomes. Mol Cell Proteomics. 2010; 9:1324–1338. [PubMed: 20224111]
19. Pisitkun T, Shen RF, Knepper MA. Identification and proteomic profiling of exosomes in human urine. Proc Natl Acad Sci USA. 2004; 101:13368–13373. [PubMed: 15326289]
20. Choi DS, Park JO, Jang SC, Yoon YJ, et al. Proteomic analysis of microvesicles derived from human colorectal cancer ascites. Proteomics. 2011; 11:2745–2751. [PubMed: 21630462]
21. Choi DS, Yang JS, Choi EJ, Jang SC, et al. The Protein Interaction Network of Extracellular Vesicles Derived from Human Colorectal Cancer Cells. J Proteome Res. 2012; 11:1144–1151. [PubMed: 22149170]
22. Gonzalez-Begne M, Lu B, Han X, Hagen FK, et al. Proteomic Analysis of Human Parotid Gland Exosomes by Multidimensional Protein Identification Technology (MudPIT). J Proteome Res. 2009; 8:1304–1314. [PubMed: 19199708]
23. Choi DS, Lee JM, Park GW, Lim HW, et al. Proteomic Analysis of Microvesicles Derived from Human Colorectal Cancer Cells. J Proteome Res. 2007; 6:4646–4655. [PubMed: 17956143]
24. Looze C, Yui D, Leung L, Ingham M, et al. Proteomic profiling of human plasma exosomes identifies PPARγ as an exosome-associated protein. Biochem Biophys Res Commun. 2009; 378:433–438. [PubMed: 19028452]
25. Hegmans JPJJ, Bard MPL, Hemmes A, Luider TM, et al. Proteomic Analysis of Exosomes Secreted by Human Mesothelioma Cells. The American Journal of Pathology. 2010; 164:1807–1815. [PubMed: 15111327]
26. Van Niel G, Raposo G, Candalh C, Boussac M, et al. Intestinal Epithelial Cells Secrete Exosome-like Vesicles. Gastroenterology. 2001; 121:337–349. [PubMed: 11487543]
27. Atay S, Gercel-Taylor C, Kesimer M, Taylor DD. Morphologic and proteomic characterization of exosomes released by cultured extravillous trophoblast cells. Exp Cell Res. 2011; 317:1192–1202. [PubMed: 21276792]
28. Adamczyk KA, Klein-Scory S, Tehrani MM, Warnken U, et al. Characterization of soluble and exosomal forms of the EGFR released from pancreatic cancer cells. Life Sci. 2011; 89:304–312. [PubMed: 21763319]
29. Stamer WD, Hoffman EA, Luther JM, Hachey DL, Schey KL. Protein profile of exosomes from trabecular meshwork cells. J Proteomics. 2011; 74:796–804. [PubMed: 21362503]
30. Mathivanan S, Fahner CJ, Reid GE, Simpson RJ. ExoCarta 2012: database of exosomal proteins, RNA and lipids. Nucleic Acids Res. 2012; 40:D1241–4. [PubMed: 21989406]
31. Mathivanan S, Simpson RJ. ExoCarta: A compendium of exosomal proteins and RNA. Proteomics. 2009; 9:4997–5000. [PubMed: 19810033]
32. Shapiro JP, Biswas S, Merchant AS, Satoskar A, et al. A quantitative proteomic workflow for characterization of frozen clinical biopsies: laser capture microdissection coupled with label-free mass spectrometry. J Proteomics. 2012; 77:433–440. [PubMed: 23022584]
33. Satoskar AA, Shapiro JP, Bott CN, Song H, et al. Characterization of glomerular diseases using proteomic analysis of laser capture microdissected glomeruli. Mod Pathol. 2012; 25:709–721. [PubMed: 22282304]
34. Goldman-Leikin RE, Salwen HR, Herst CV. Characterization of a novel myeloma cell line, MM. 1. J Lab Clin Med. 1989; 113:335–345. [PubMed: 2926241]

35. Nilsson K, Bennich H, Johansson SG, Pontén J. Established immunoglobulin producing myeloma (IgE) and lymphoblastoid (IgG) cell lines from an IgE myeloma patient. Clin Exp Immunol. 1970; 7:477–489. [PubMed: 4097745]
36. Théry C, Amigorena S, Raposo G, Clayton A. Isolation and characterization of exosomes from cell culture supernatants and biological fluids. Curr Protoc Cell Biol. 2006; Chapter 3(Unit 3.22)
37. Xu H, Freitas MA. A mass accuracy sensitive probability based scoring algorithm for database searching of tandem mass spectrometry data. BMC Bioinformatics. 2007; 8:133. [PubMed: 17448237]
38. Xu H, Yang L, Freitas MA. A robust linear regression based algorithm for automated evaluation of peptide identifications from shotgun proteomics by use of reversed-phase liquid chromatography retention time. BMC Bioinformatics. 2008; 9:347. [PubMed: 18713471]
39. Xu H, Zhang L, Freitas MA. Identification and characterization of disulfide bonds in proteins and peptides from tandem MS data by use of the MassMatrix MS/MS search engine. J Proteome Res. 2008; 7:138–144. [PubMed: 18072732]
40. Xu H, Freitas MA. Monte carlo simulation-based algorithms for analysis of shotgun proteomic data. J Proteome Res. 2008; 7:2605–2615. [PubMed: 18543962]
41. Zhang B, Chambers MC, Tabb DL. Proteomic parsimony through bipartite graph analysis improves accuracy and transparency. J Proteome Res. 2007; 6:3549–3557. [PubMed: 17676885]
42. Liu H, Sadygov RG, Yates JR. A model for random sampling and estimation of relative protein abundance in shotgun proteomics. Anal Chem. 2004; 76:4193–4201. [PubMed: 15253663]
43. Colinge J, Chiappe D, Lagache S, Moniatte M, Bougueleret L. Differential proteomics via probabilistic peptide identification scores. Anal Chem. 2005; 77:596–606. [PubMed: 15649059]
44. Robinson MDM, McCarthy DJD, Smyth GKG. edgeR: a Bioconductor package for differential expression analysis of digital gene expression data. Audio, Transactions of the IRE Professional Group on. 2010; 26:139–140.
45. Robinson MDM, Smyth GKG. Moderated statistical tests for assessing differences in tag abundance. Bioinformatics. 2007; 23:2881–2887. [PubMed: 17881408]
46. Robinson MDM, Smyth GKG. Small-sample estimation of negative binomial dispersion, with applications to SAGE data. Biostatistics. 2008; 9:321–332. [PubMed: 17728317]
47. Benjamini Y, Hochberg Y. Controlling the false discovery rate: a practical and powerful approach to multiple testing. Journal of the Royal Statistical Society Series B (Methodological). 1995:289–300.
48. Hulsen T, de Vlieg J, Alkema W. BioVenn - a web application for the comparison and visualization of biological lists using area-proportional Venn diagrams. BMC Genomics. 2008; 9:488. [PubMed: 18925949]
49. Thomas PD, Kejariwal A, Campbell MJ, Mi H, et al. PANTHER: a browsable database of gene products organized by biological function, using curated protein family and subfamily classification. Nucleic Acids Res. 2003; 31:334–341. [PubMed: 12520017]
50. Mi H, Dong Q, Muruganujan A, Gaudet P, et al. PANTHER version 7: improved phylogenetic trees, orthologs and collaboration with the Gene Ontology Consortium. Nucleic Acids Res. 2010; 38:D204–10. [PubMed: 20015972]
51. Elmore S. Apoptosis: a review of programmed cell death. Toxicol Pathol. 2007; 35:495–516. [PubMed: 17562483]
52. Mathivanan S, Ji H, Simpson RJ. Exosomes: Extracellular organelles important in intercellular communication. J Proteomics. 2010; 73:1907–1920. [PubMed: 20601276]
53. Cicero, A.; Raposo, G. Emerging Concepts of Tumor Exosome–Mediated Cell-Cell Communication. Zhang, H-G., editor. Springer; 2012.
54. Février B, Raposo G. Exosomes: endosomal-derived vesicles shipping extracellular messages. Curr Opin Cell Biol. 2004; 16:415–421. [PubMed: 15261674]
55. Klein, B.; Seckinger, A.; Moehler, T.; Hose, D. Multiple Myeloma. Moehler, T.; Goldschmidt, H., editors. Vol. 183. Springer Berlin Heidelberg; Berlin, Heidelberg: 2011. p. 39-86.
56. Srivastava M, Pollard HB. Molecular dissection of nucleolin's role in growth and cell proliferation: new insights. FASEB J. 1999; 13:1911–1922. [PubMed: 10544174]

57. Pickering BF, Yu D, Van Dyke MW. Nucleolin protein interacts with microprocessor complex to affect biogenesis of microRNAs 15a and 16. J Biol Chem. 2011; 286:44095–44103. [PubMed: 22049078]
58. Martello G, Rosato A, Ferrari F, Manfrin A, et al. A MicroRNA targeting dicer for metastasis control. Cell. 2010; 141:1195–1207. [PubMed: 20603000]
59. Di Leva G, Croce CM. Roles of small RNAs in tumor formation. Trends Mol Med. 2010; 16:257–267. [PubMed: 20493775]
60. Pichiorri F, Palmieri D, De Luca L, Consiglio J, et al. In vivo NCL targeting affects breast cancer aggressiveness through miRNA regulation. Journal of Experimental Medicine. 2013; 210:951–968. [PubMed: 23610125]
61. Raposo G, Nijman HW, Stoorvogel W, Liejendekker R, et al. B lymphocytes secrete antigen-presenting vesicles. J Exp Med. 1996; 183:1161–1172. [PubMed: 8642258]
62. Escola JM, Kleijmeer MJ, Stoorvogel W, Griffith JM, et al. Selective enrichment of tetraspan proteins on the internal vesicles of multivesicular endosomes and on exosomes secreted by human B-lymphocytes. J Biol Chem. 1998; 273:20121–20127. [PubMed: 9685355]
63. Garrido F, Cabrera T, Aptsiauri N. “Hard” and “soft” lesions underlying the HLA class I alterations in cancer cells: implications for immunotherapy. Int J Cancer. 2010; 127:249–256. [PubMed: 20178101]
64. Lee CT, Mace T, Repasky EA. Hypoxia-driven immunosuppression: a new reason to use thermal therapy in the treatment of cancer? Int J Hyperthermia. 2010; 26:232–246. [PubMed: 20388021]

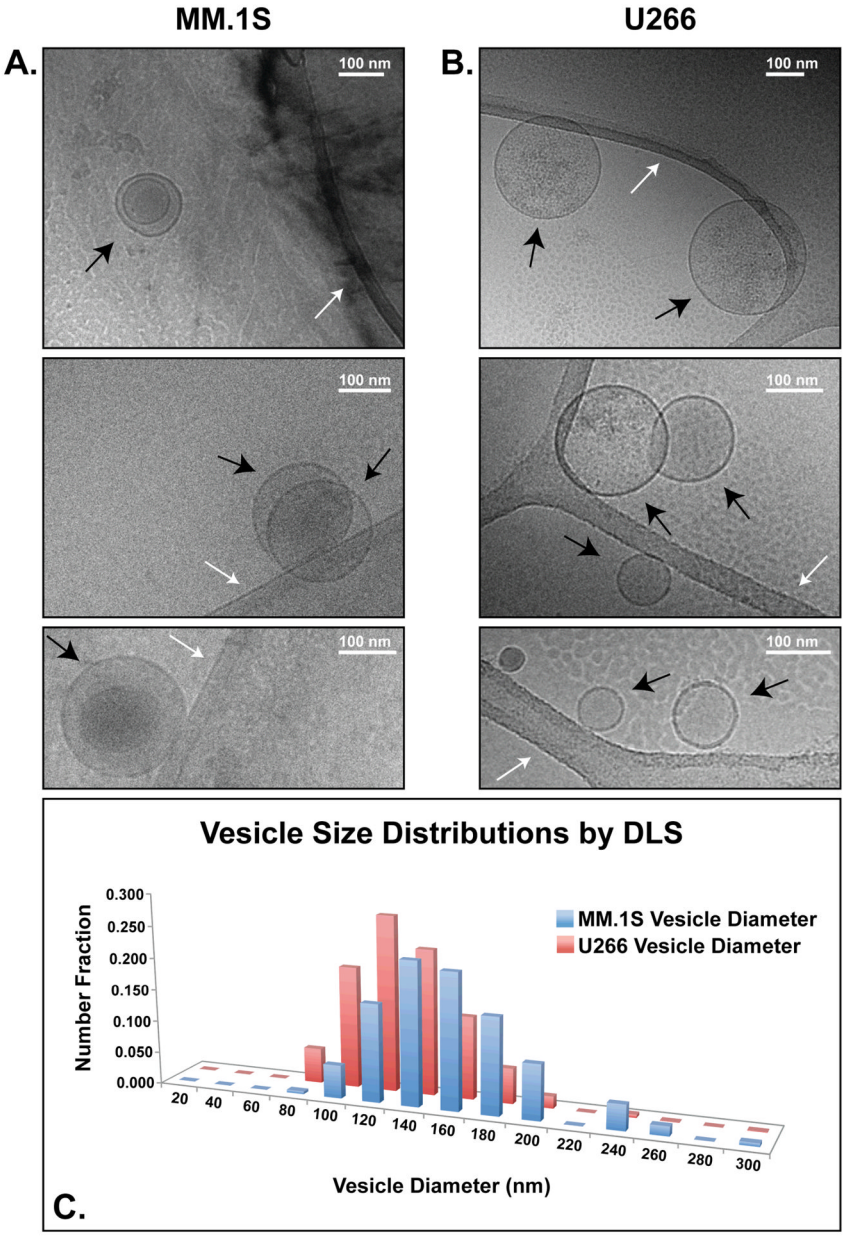

Figure 1.

Cryo-transmission electron microscopy (cryo-TEM) images of the **A)** MM.1S cell-derived extracellular vesicles and **B)** U266 cell-derived extracellular vesicles, indicated by the black. The cryo-TEM carbon support grids (white arrows) are also seen these images. **C)** Number distributions of MM.1S and U266 extracellular vesicle diameters derived from Dynamic Light Scattering (DLS) measurements.

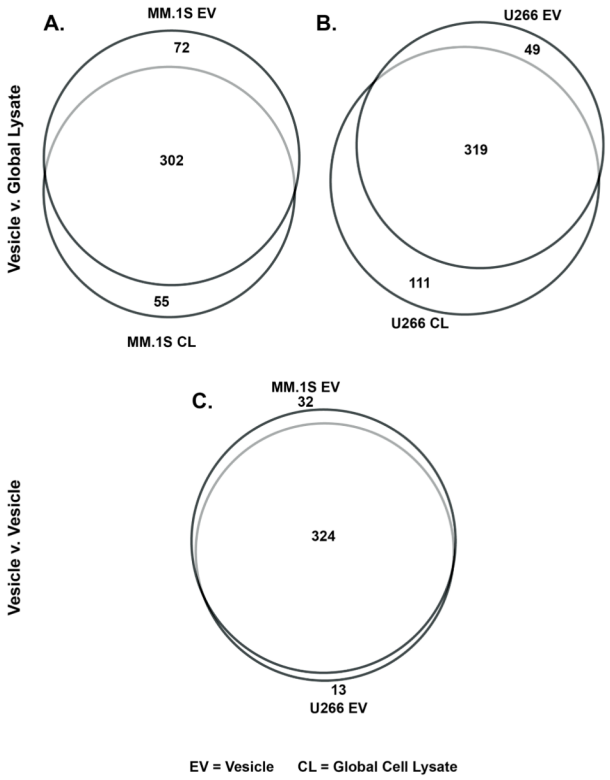

Figure 2.

Venn diagram renderings of overlapping and unique protein identifications. **A)** MM.1S vesicles (EV) v. global cell lysate (CL). **B)** U266 vesicles (EV) v. global cell lysate (CL). **C)** MM.1S vesicles (EV) v. U266 vesicles (EV). Data shows many overlapping protein identifications while also harboring unique IDs in each comparison.

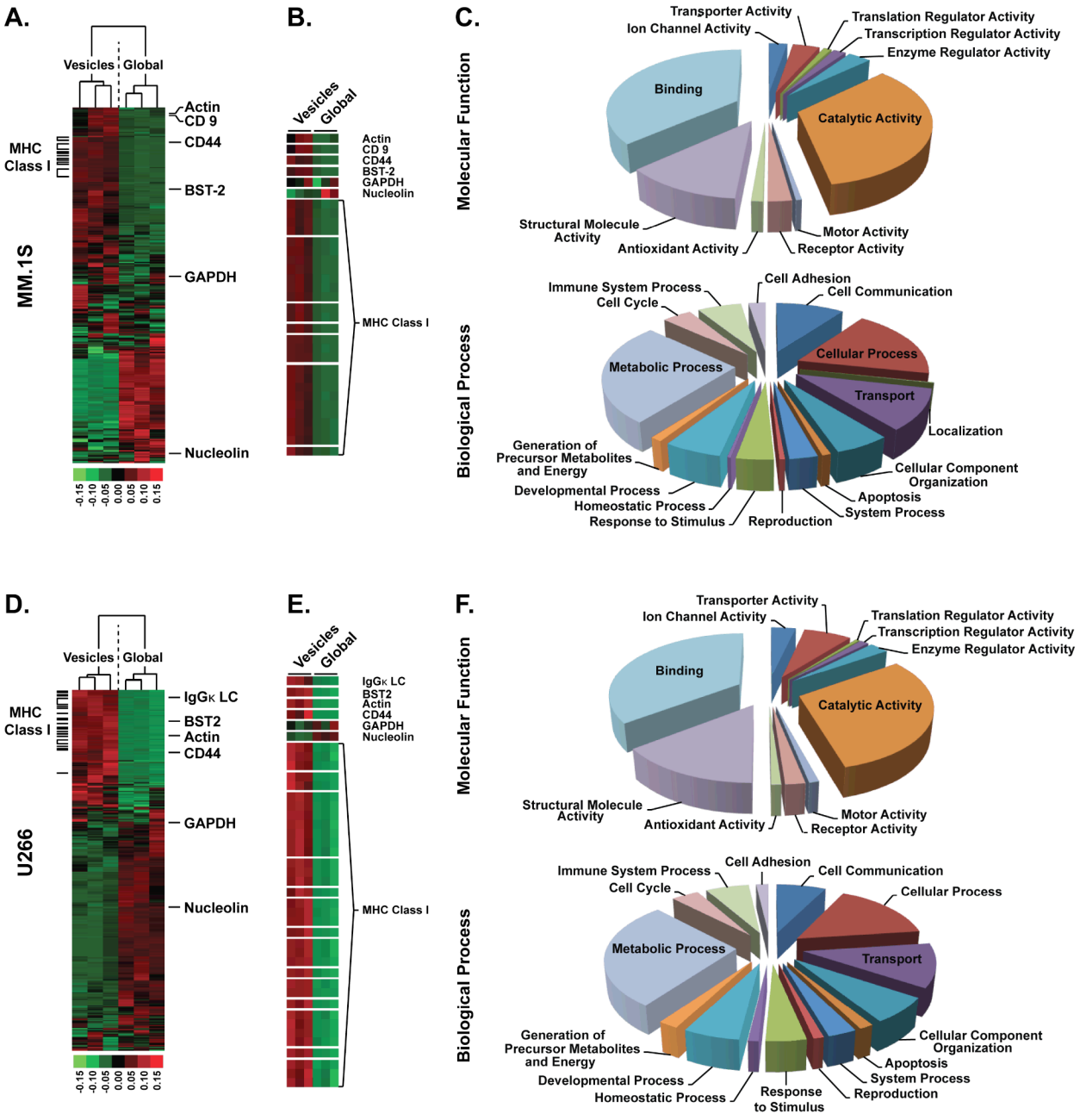

Figure 3.

Clustering of LC-MS/MS spectral counts and pie chart illustrations of the PANTHER gene ontology annotations for molecular function and biological process for those proteins with significantly different abundances between the cell line vesicles when compared to the parent cell lysate. **A)** Clustering of spectral count data for the MM.1S vesicles and parent cell lysate. **B)** Enlarged clustering of spectral count data for those proteins selected for validation from MM.1S cell line. **C)** PANTHER gene ontological annotations for the molecular function and biological process for proteins with statistically different abundances from the MM.1S cell line. **D)** Clustering of spectral count data for the U266 vesicles and parent cell lysate. **E)** Enlarged clustering of spectral count data for those proteins selected for validation from the U266 cell line. **F)** PANTHER gene ontological annotations for the

molecular function and biological process for proteins with statistically different abundances from the U266 cell line. Results suggest variable abundance of specific proteins, which can confer different potential biological processes and molecular functions.

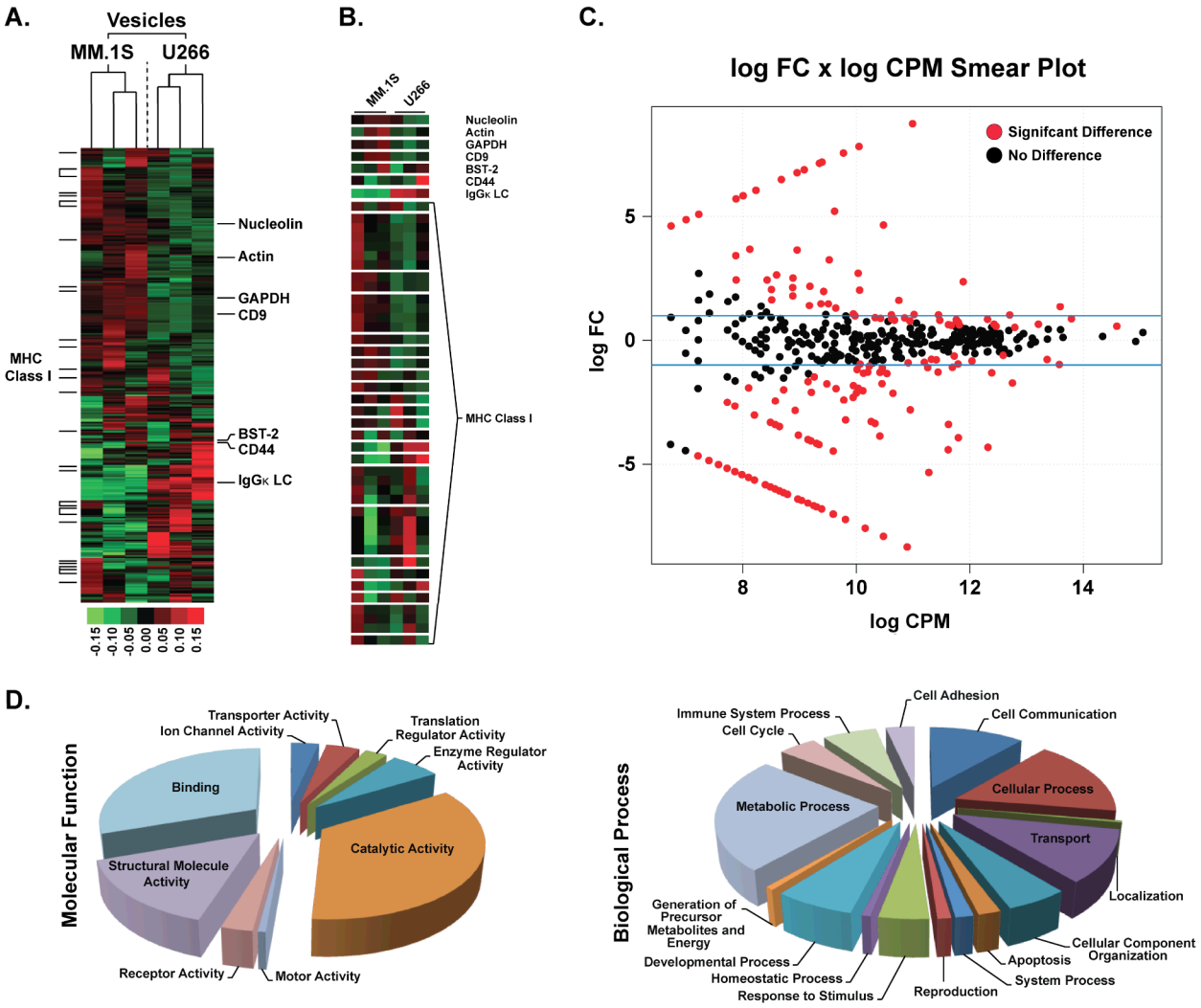

Figure 4.

EdgeR label-free analysis for differentially expressed proteins from the MM.1S derived vesicles and the U266 derived vesicles. **A)** Hierarchal clustering of LC-MS/MS spectral count data. **B)** Enlarged clustering of spectral count data for those proteins selected for validation. **C)** Smear plot of the log fold change (log FC) by log counts-per-million (log CPM) for the vesicle data from each cell line. **D)** Pie chart illustrations of the PANTHER gene ontology annotations for molecular function and biological process for those proteins differentially expressed between the MM derived vesicles. Data suggests vesicular protein abundance distinguishes between the cells of origin allowing for differential functional potential.

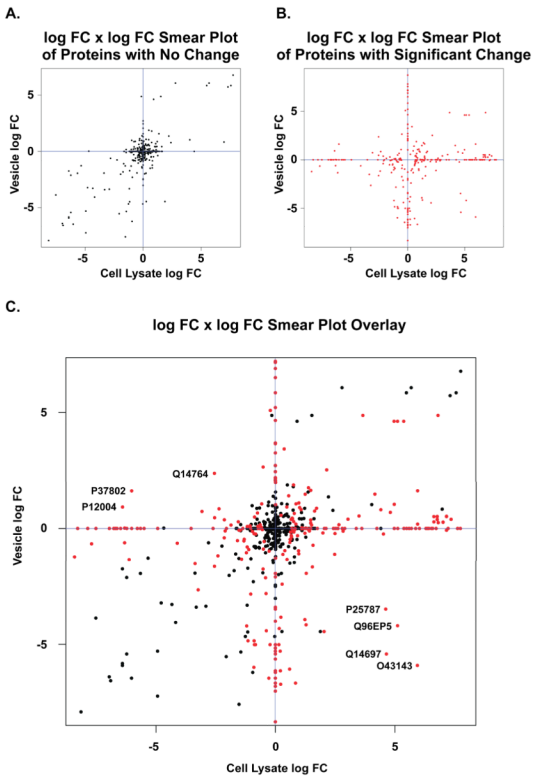

Figure 5.

Smear plot of log fold change by log fold change for the vesicles and global cell lysates. **A)** Proteins with no significant change in abundance between vesicles and global lysates changes in the same direction. **B)** Proteins with significant abundance differences in opposite directions between the vesicle and global lysate samples. **C)** Overlay of **A & B**. Those proteins with the greatest independent differences in abundance are labeled with Uniprot Accession numbers.

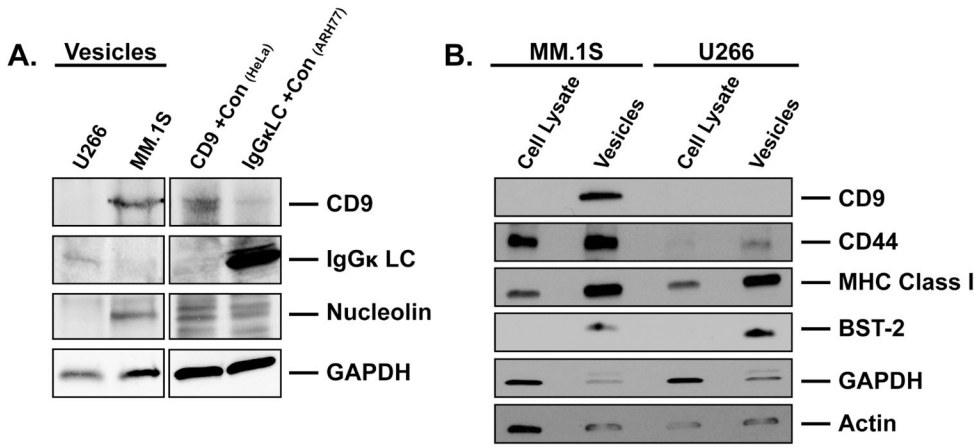

Figure 6.

Validation of protein identifications and spectral count relative quantitation from the proteomic analysis of the MM.1S and U266 derived vesicles and global cell lysates by immunoblot. **A)** Immunoblot of vesicle identified proteins. Blot was probed for CD9, IgGκ LC, Nucleolin and GAPDH. **B)** Immunoblot for comparison of protein relative abundance between vesicles and cell lysates. Blots were probed for CD9, CD44, MHC Class I, BST-2, GAPDH and Actin. Data confirms the LC-MS/MS protein identifications and relative abundances observed in the data sets. HeLa (CD9) and ARH77 (IgGκ LC) global lysates were used as positive controls.

Table 1

List of proteins with differential abundances based on the label-free analysis of the vesicles derived from both the MM.1S and U266 cell lines.

edgeR Analysis for Variably Expressed Proteins in the Cell Line Derived Vesicles										
	MM1S Vesicle Spectral Count			U266 Vesicle Spectral Count			Statistics			
Identification	**Replicate 1**	**Replicate 2**	**Replicate 3**	**Replicate 1**	**Replicate 2**	**Replicate 3**	**logFC**	**logCPM**	**PValue**	**BH.mt.adj**
sp|B9A064|IGLL5_HUMAN Immunoglobulin lambda-like polypeptide 5 OS=Homo sapiens GN=IGLL5 PE=2 SV=2	103	57	88	5	3	1	−4.27614	12.41465	3.01E-26	−1
sp|P01834|IGKC_HUMAN Ig kappa chain C region OS=Homo sapiens GN=IGKC PE=1 SV=1	0	0	0	34	36	21	8.76905	11.11035	2.20E-23	1
sp|P0CG04|LAC1_HUMAN Ig lambda-1 chain C regions OS=Homo sapiens GN=IGLC1 PE=1 SV=1	76	36	57	5	3	0	−3.88945	11.89555	1.41E-19	−1
sp|P55072|TERA_HUMAN Transitional endoplasmic reticulum ATPase OS=Homo sapiens GN=VCP PE=1 SV=4	46	48	56	5	0	0	−4.37390	11.71447	1.41E-19	−1
sp|P29401|TKT_HUMAN Transketolase OS=Homo sapiens GN=TKT PE=1 SV=3	42	34	44	0	2	0	−5.29025	11.37466	6.73E-19	−1
sp|P80723|BASP1_HUMAN Brain acid soluble protein 1 OS=Homo sapiens GN=BASP1 PE=1 SV=2	30	27	36	0	0	0	−8.32492	10.99411	4.02E-18	−1
sp|P33241|LSP1_HUMAN Lymphocyte-specific protein 1 OS=Homo sapiens GN=LSP1 PE=1 SV=1	0	0	3	9	15	37	4.69387	10.59540	3.17E-16	1
sp|P07195|LDHB_HUMAN L-lactate dehydrogenase B chain OS=Homo sapiens GN=LDHB PE=1 SV=2	51	50	44	6	3	1	−3.35433	11.71943	2.82E-15	−1
sp|P22732|GTR5_HUMAN Solute carrier family 2; facilitated glucose transporter member 5 OS=Homo sapiens GN=SLC2A5 PE=1 SV=1	0	0	0	12	15	21	7.84918	10.16316	3.84E-14	1
sp|P52566|GDIR2_HUMAN Rho GDP-dissociation inhibitor 2 OS=Homo sapiens GN=ARHGDIB PE=1 SV=3	21	24	24	0	0	0	−7.89585	10.57644	4.87E-14	−1
sp|Q14764|MVP_HUMAN Major vault protein OS=Homo sapiens GN=MVP PE=1 SV=4	16	5	14	22	76	37	2.41451	11.99966	2.92E-13	1
sp|P23634|AT2B4_HUMAN Plasma membrane calcium-transporting ATPase 4 OS=Homo sapiens GN=ATP2B4 PE=1 SV=2	0	0	0	10	17	13	7.58739	9.88687	6.32E-12	1
sp|Q15181|IPYR_HUMAN Inorganic pyrophosphatase OS=Homo sapiens GN=PPA1 PE=1 SV=2	17	17	21	0	0	0	−7.57023	10.25697	1.61E-11	−1
sp|Q9H4M9|EHD1_HUMAN EH domain-containing protein 1 OS=Homo sapiens GN=EHD1 PE=1 SV=2	0	0	1	11	12	12	5.24615	9.73067	5.28E-11	1
sp|P49327|FAS_HUMAN Fatty acid synthase OS=Homo sapiens GN=FASN PE=1 SV=3	32	21	10	0	3	0	−3.82508	10.51397	2.83E-10	−1

edgeR Analysis for Variably Expressed Proteins in the Cell Line Derived Vesicles

	MM1S Vesicle Spectral Count			U266 Vesicle Spectral Count			Statistics			
Identification	**Replicate 1**	**Replicate 2**	**Replicate 3**	**Replicate 1**	**Replicate 2**	**Replicate 3**	**logFC**	**logCPM**	**PValue**	**BH.mt.adj**
sp|Q16222|UAP1_HUMAN UDP-N-acetylhexosamine pyrophosphorylase OS=Homo sapiens GN=UAP1 PE=1 SV=3	0	0	0	11	9	10	7.17485	9.46362	2.43E-09	1
sp|O00764|PDXK_HUMAN Pyridoxal kinase OS=Homo sapiens GN=PDXK PE=1 SV=1	13	16	14	0	0	0	−7.21725	9.90993	2.62E-09	−1
sp|Q96KP4|CNDP2_HUMAN Cytosolic non-specific dipeptidase OS=Homo sapiens GN=CNDP2 PE=1 SV=2	39	25	23	6	1	2	−2.76801	11.05055	3.27E-09	−1
sp|P13639|EF2_HUMAN Elongation factor 2 OS=Homo sapiens GN=EEF2 PE=1 SV=4	88	89	99	19	25	18	−1.67430	12.84760	3.96E-09	−1
sp|P61160|ARP2_HUMAN Actin-related protein 2 OS=Homo sapiens GN=ACTR2 PE=1 SV=1	18	15	25	0	4	0	−3.31501	10.43081	1.21E-08	−1
sp|P14618|KPYM_HUMAN Pyruvate kinase isozymes M1/M2 OS=Homo sapiens GN=PKM PE=1 SV=4	56	67	67	116	138	107	1.40132	13.70675	1.67E-08	1
sp|P04080|CYTB_HUMAN Cystatin-B OS=Homo sapiens GN=CSTB PE=1 SV=2	17	18	20	2	2	0	−3.23878	10.36238	2.91E-08	−1
sp|P05556|ITB1_HUMAN Integrin beta-1 OS=Homo sapiens GN=ITGB1 PE=1 SV=2	0	0	0	5	10	10	6.91382	9.19461	4.15E-08	1
sp|Q8WWI5|CTL1_HUMAN Choline transporter-like protein 1 OS=Homo sapiens GN=SLC44A1 PE=1 SV=1	21	10	6	0	0	0	−7.00201	9.69324	6.28E-08	−1
sp|P27701|CD82_HUMAN CD82 antigen OS=Homo sapiens GN=CD82 PE=1 SV=1	10	14	13	0	0	0	−7.00201	9.69762	6.28E-08	−1
sp|O15247|CLIC2_HUMAN Chloride intracellular channel protein 2 OS=Homo sapiens GN=CLIC2 PE=1 SV=3	4	10	15	0	0	0	−6.65364	9.35311	1.32E-07	−1
sp|P43358|MAGA4_HUMAN Melanoma-associated antigen 4 OS=Homo sapiens GN=MAGEA4 PE=1 SV=2	0	0	0	8	11	4	6.79456	9.06785	1.32E-07	1
sp|P62244|RS15A_HUMAN 40S ribosomal protein S15a OS=Homo sapiens GN=RPS15A PE=1 SV=2	8	9	12	0	0	0	−6.65364	9.35150	2.37E-07	−1
sp|Q01650|LAT1_HUMAN Large neutral amino acids transporter small subunit 1 OS=Homo sapiens GN=SLC7A5 PE=1 SV=2	5	3	0	9	13	18	2.75461	10.14575	2.60E-07	1
sp|Q16555|DPYL2_HUMAN Dihydropyrimidinase-related protein 2 OS=Homo sapiens GN=DPYSL2 PE=1 SV=1	6	8	13	0	0	0	−6.55160	9.25040	4.27E-07	−1
sp|P21926|CD9_HUMAN CD9 antigen OS=Homo sapiens GN=CD9 PE=1 SV=4	8	11	13	0	0	0	−6.79431	9.49176	5.49E-07	−1
sp|Q01105|SET_HUMAN Protein SET OS=Homo sapiens GN=SET PE=1 SV=3	16	8	12	0	1	0	−4.43095	9.69622	8.01E-07	−1

edgeR Analysis for Variably Expressed Proteins in the Cell Line Derived Vesicles

	MM1S Vesicle Spectral Count			U266 Vesicle Spectral Count			Statistics			
Identification	**Replicate 1**	**Replicate 2**	**Replicate 3**	**Replicate 1**	**Replicate 2**	**Replicate 3**	**logFC**	**logCPM**	**PValue**	**BH.mt.adj**
sp|O00161|SNP23_HUMAN Synaptosomal-associated protein 23 OS=Homo sapiens GN=SNAP23 PE=1 SV=1	1	3	0	9	16	5	3.29231	9.63398	9.51E-07	1
sp|P31350|RIR2_HUMAN Ribonucleoside-diphosphate reductase subunit M2 OS=Homo sapiens GN=RRM2 PE=1 SV=1	9	7	9	0	0	0	−6.44180	9.13949	1.40E-06	−1
sp|P37837|TALDO_HUMAN Transaldolase OS=Homo sapiens GN=TALDO1 PE=1 SV=2	7	6	12	0	0	0	−6.44180	9.14012	1.40E-06	−1
sp|O00410|IPO5_HUMAN Importin-5 OS=Homo sapiens GN=IPO5 PE=1 SV=4	8	9	8	0	0	0	−6.44180	9.14013	1.40E-06	−1
sp|P49773|HINT1_HUMAN Histidine triad nucleotide-binding protein 1 OS=Homo sapiens GN=HINT1 PE=1 SV=2	10	9	11	0	0	0	−6.70207	9.39899	1.65E-06	−1
sp|P02768|ALBU_HUMAN Serum albumin OS=Homo sapiens GN=ALB PE=1 SV=2	24	0	0	0	0	0	−6.38360	9.07465	2.55E-06	−1
sp|P27105|STOM_HUMAN Erythrocyte band 7 integral membrane protein OS=Homo sapiens GN=STOM PE=1 SV=3	0	0	0	3	9	7	6.52166	8.79041	2.55E-06	1
sp|P29692|EF1D_HUMAN Elongation factor 1-delta OS=Homo sapiens GN=EEF1D PE=1 SV=5	13	9	18	3	0	0	−3.17354	9.91472	2.55E-06	−1
sp|P62330|ARF6_HUMAN ADP-ribosylation factor 6 OS=Homo sapiens GN=ARF6 PE=1 SV=2	0	0	2	7	6	8	3.68737	9.06863	4.98E-06	1
sp|P13796|PLSL_HUMAN Plastin-2 OS=Homo sapiens GN=LCP1 PE=1 SV=6	62	56	83	25	33	2	−1.26454	12.48648	6.55E-06	−1
sp|Q01518|CAP1_HUMAN Adenylyl cyclase-associated protein 1 OS=Homo sapiens GN=CAP1 PE=1 SV=5	19	18	29	3	6	2	−2.08745	10.74754	8.81E-06	−1
sp|P17858|K6PL_HUMAN 6-phosphofructokinase; liver type OS=Homo sapiens GN=PFKL PE=1 SV=6	14	9	7	0	1	0	−4.17023	9.44566	1.07E-05	−1
sp|P63244|GBLP_HUMAN Guanine nucleotide-binding protein subunit beta-2-like 1 OS=Homo sapiens GN=GNB2L1 PE=1 SV=3	6	8	7	0	0	0	−6.19342	8.89210	1.58E-05	−1
sp|Q9BY67|CADM1_HUMAN Cell adhesion molecule 1 OS=Homo sapiens GN=CADM1 PE=1 SV=2	10	6	5	0	0	0	−6.19342	8.89027	1.58E-05	−1
sp|Q13576|IQGA2_HUMAN Ras GTPase-activating-like protein IQGAP2 OS=Homo sapiens GN=IQGAP2 PE=1 SV=4	5	9	15	0	1	0	−4.12179	9.40235	1.80E-05	−1
sp|Q99959|PKP2_HUMAN Plakophilin-2 OS=Homo sapiens GN=PKP2 PE=1 SV=2	2	2	8	5	13	19	2.07475	10.17041	2.11E-05	1
sp|P10909|CLUS_HUMAN Clusterin OS=Homo sapiens GN=CLU PE=1 SV=1	10	6	4	0	0	0	−6.12402	8.82060	2.92E-05	−1

Proteomics. Author manuscript; available in PMC 2014 October 01.

edgeR Analysis for Variably Expressed Proteins in the Cell Line Derived Vesicles

	MM1S Vesicle Spectral Count			U266 Vesicle Spectral Count			Statistics			
Identification	**Replicate 1**	**Replicate 2**	**Replicate 3**	**Replicate 1**	**Replicate 2**	**Replicate 3**	**logFC**	**logCPM**	**PValue**	**BH.mt.adj**
sp|P13010|XRCC5_HUMAN X-ray repair cross-complementing protein 5 OS=Homo sapiens GN=XRCC5 PE=1 SV=3	11	5	4	0	0	0	−6.12402	8.82008	2.92E-05	−1
sp|O15144|ARPC2_HUMAN Actin-related protein 2/3 complex subunit 2 OS=Homo sapiens GN=ARPC2 PE=1 SV=1	7	5	7	0	0	0	−6.05110	8.74838	2.92E-05	−1
sp|Q04760|LGUL_HUMAN Lactoylglutathione lyase OS=Homo sapiens GN=GLO1 PE=1 SV=4	9	6	5	0	0	0	−6.12402	8.82100	2.92E-05	−1
sp|P09874|PARP1_HUMAN Poly [ADP-ribose] polymerase 1 OS=Homo sapiens GN=PARP1 PE=1 SV=4	7	8	12	1	0	0	−4.01976	9.30380	3.05E-05	−1
sp|P37802|TAGL2_HUMAN Transgelin-2 OS=Homo sapiens GN=TAGLN2 PE=1 SV=3	7	7	10	19	18	18	1.66118	10.86215	3.94E-05	1
sp|P15121|ALDR_HUMAN Aldose reductase OS=Homo sapiens GN=AKR1B1 PE=1 SV=3	10	10	6	1	0	0	−3.96591	9.25116	5.15E-05	−1
sp|Q96GU1|GGEE1_HUMAN G antigen family E member 1 OS=Homo sapiens GN=PAGE5 PE=2 SV=2	0	0	0	8	3	3	6.08668	8.34436	5.43E-05	1
sp|P18124|RL7_HUMAN 60S ribosomal protein L7 OS=Homo sapiens GN=RPL7 PE=1 SV=1	8	9	1	0	0	0	−5.97431	8.67127	5.43E-05	−1
sp|P08195|4F2_HUMAN 4F2 cell-surface antigen heavy chain OS=Homo sapiens GN=SLC3A2 PE=1 SV=3	57	32	32	51	64	67	1.06381	12.81645	5.81E-05	1
sp|Q16543|CDC37_HUMAN Hsp90 co-chaperone Cdc37 OS=Homo sapiens GN=CDC37 PE=1 SV=1	0	0	0	7	7	0	6.08668	8.34040	0.00010	1
sp|P29350|PTN6_HUMAN Tyrosine-protein phosphatase non-receptor type 6 OS=Homo sapiens GN=PTPN6 PE=1 SV=1	3	4	10	0	0	0	−5.89320	8.59088	0.00010	−1
sp|P16949|STMN1_HUMAN Stathmin OS=Homo sapiens GN=STMN1 PE=1 SV=3	12	9	16	2	3	0	−2.36304	9.88413	0.00010	−1
sp|P15311|EZRI_HUMAN Ezrin OS=Homo sapiens GN=EZR PE=1 SV=4	58	96	116	102	107	156	0.91090	13.90258	0.00011	1
sp|P08133|ANXA6_HUMAN Annexin A6 OS=Homo sapiens GN=ANXA6 PE=1 SV=3	147	145	140	85	57	21	−0.92859	13.67668	0.00013	−1
sp|P63241|IF5A1_HUMAN Eukaryotic translation initiation factor 5A-1 OS=Homo sapiens GN=EIF5A PE=1 SV=2	14	13	14	0	3	3	−2.25669	10.04660	0.00013	−1
sp|P14324|FPPS_HUMAN Farnesyl pyrophosphate synthase OS=Homo sapiens GN=FDPS PE=1 SV=4	7	4	5	0	0	0	−5.80725	8.50256	0.00019	−1
sp|P26641|EF1G_HUMAN Elongation factor 1-gamma OS=Homo sapiens GN=EEF1G PE=1 SV=3	14	13	18	7	1	0	−1.98724	10.21911	0.00022	−1

edgeR Analysis for Variably Expressed Proteins in the Cell Line Derived Vesicles

	MM1S Vesicle Spectral Count			U266 Vesicle Spectral Count			Statistics			
Identification	**Replicate 1**	**Replicate 2**	**Replicate 3**	**Replicate 1**	**Replicate 2**	**Replicate 3**	**logFC**	**logCPM**	**PValue**	**BH.mt.adj**
sp|P41219|PERI_HUMAN Peripherin OS=Homo sapiens GN=PRPH PE=1 SV=2	10	7	6	1	0	0	−3.79111	9.08295	0.00025	−1
sp|P59998|ARPC4_HUMAN Actin-related protein 2/3 complex subunit 4 OS=Homo sapiens GN=ARPC4 PE=1 SV=3	20	11	11	2	2	3	−2.07577	10.10553	0.00030	−1
sp|P33908|MA1A1_HUMAN Mannosyl-oligosaccharide 1;2-alpha-mannosidase IA OS=Homo sapiens GN=MAN1A1 PE=1 SV=3	0	0	0	0	11	1	5.86783	8.11405	0.00036	1
sp|P0CV98|TSPY3_HUMAN Testis-specific Y-encoded protein 3 OS=Homo sapiens GN=TSPY3 PE=3 SV=1	0	0	0	3	7	2	5.86783	8.11676	0.00036	1
sp|P15153|RAC2_HUMAN Ras-related C3 botulinum toxin substrate 2 OS=Homo sapiens GN=RAC2 PE=1 SV=1	18	19	18	2	7	3	−1.70240	10.55449	0.00043	−1
sp|P25787|PSA2_HUMAN Proteasome subunit alpha type-2 OS=Homo sapiens GN=PSMA2 PE=1 SV=2	9	6	3	0	1	0	−3.44247	8.74932	0.00046	−1
sp|P31949|S10AB_HUMAN Protein S100-A11 OS=Homo sapiens GN=S100A11 PE=1 SV=2	13	11	18	1	3	4	−1.88837	10.13833	0.00064	−1
sp|Q08431|MFGM_HUMAN Lactadherin OS=Homo sapiens GN=MFGE8 PE=1 SV=2	34	34	34	9	9	13	−1.23595	11.54076	0.00066	−1
sp|Q30134|2B18_HUMAN HLA class II histocompatibility antigen; DRB1–8 beta chain OS=Homo sapiens GN=HLA-DRB1 PE=1 SV=2	8	3	3	0	0	0	−5.61828	8.31090	0.00067	−1
sp|Q01534|TSPY1_HUMAN Testis-specific Y-encoded protein 1 OS=Homo sapiens GN=TSPY1 PE=1 SV=4	0	0	0	3	6	2	5.74454	7.99047	0.00067	1
sp|Q9BZQ8|NIBAN_HUMAN Protein Niban OS=Homo sapiens GN=FAM129A PE=1 SV=1	7	0	1	6	13	5	2.02263	9.53512	0.00084	1
sp|P55327|TPD52_HUMAN Tumor protein D52 OS=Homo sapiens GN=TPD52 PE=1 SV=2	1	2	1	13	5	0	2.56199	8.99457	0.00093	1
sp|P01111|RASN_HUMAN GTPase NRas OS=Homo sapiens GN=NRAS PE=1 SV=1	3	0	3	3	10	8	2.23003	9.29311	0.00121	1
sp|P23284|PPIB_HUMAN Peptidyl-prolyl cis-trans isomerase B OS=Homo sapiens GN=PPIB PE=1 SV=2	0	0	3	8	3	4	2.68506	8.70598	0.00121	1
sp|P24534|EF1B_HUMAN Elongation factor 1-beta OS=Homo sapiens GN=EEF1B2 PE=1 SV=3	3	3	7	0	0	0	−5.51362	8.20682	0.00128	−1
sp|P40925|MDHC_HUMAN Malate dehydrogenase; cytoplasmic OS=Homo sapiens GN=MDH1 PE=1 SV=4	8	12	19	2	3	3	−1.78222	10.05221	0.00130	−1
sp|Q9Y696|CLIC4_HUMAN Chloride intracellular channel protein 4 OS=Homo sapiens GN=CLIC4 PE=1 SV=4	15	12	24	21	23	33	1.06676	11.55959	0.00136	1

Proteomics. Author manuscript; available in PMC 2014 October 01.

edgeR Analysis for Variably Expressed Proteins in the Cell Line Derived Vesicles

	MM1S Vesicle Spectral Count			U266 Vesicle Spectral Count			Statistics			
Identification	**Replicate 1**	**Replicate 2**	**Replicate 3**	**Replicate 1**	**Replicate 2**	**Replicate 3**	**logFC**	**logCPM**	**PValue**	**BH.mt.adj**
sp|O14745|NHRF1_HUMAN Na(+)/H(+) exchange regulatory cofactor NHE-RF1 OS=Homo sapiens GN=SLC9A3R1 PE=1 SV=4	20	34	45	40	33	59	0.88978	12.42375	0.00143	1
sp|P52209|6PGD_HUMAN 6-phosphogluconate dehydrogenase; decarboxylating OS=Homo sapiens GN=PGD PE=1 SV=3	5	5	6	1	0	0	−3.27541	8.59232	0.00143	−1
sp|Q16720|AT2B3_HUMAN Plasma membrane calcium-transporting ATPase 3 OS=Homo sapiens GN=ATP2B3 PE=1 SV=3	0	0	1	3	5	4	3.71816	8.23361	0.00143	1
sp|P08670|VIME_HUMAN Vimentin OS=Homo sapiens GN=VIM PE=1 SV=4	44	36	38	26	9	6	−1.04462	11.79524	0.00152	−1
sp|P50995|ANX11_HUMAN Annexin A11 OS=Homo sapiens GN=ANXA11 PE=1 SV=1	7	6	5	0	0	1	−3.44247	8.75122	0.00204	−1
sp|P28838|AMPL_HUMAN Cytosol aminopeptidase OS=Homo sapiens GN=LAP3 PE=1 SV=3	9	0	3	0	0	0	−5.40078	8.08922	0.00244	−1
sp|P49720|PSB3_HUMAN Proteasome subunit beta type-3 OS=Homo sapiens GN=PSMB3 PE=1 SV=2	7	1	3	0	0	0	−5.27835	7.96545	0.00244	−1
sp|P46926|GNPI1_HUMAN Glucosamine-6-phosphate isomerase 1 OS=Homo sapiens GN=GNPDA1 PE=1 SV=1	5	1	5	0	0	0	−5.27835	7.96628	0.00244	−1
sp|Q07020|RL18_HUMAN 60S ribosomal protein L18 OS=Homo sapiens GN=RPL18 PE=1 SV=2	6	9	6	0	1	1	−2.79204	9.02624	0.00246	−1
sp|P60763|RAC3_HUMAN Ras-related C3 botulinum toxin substrate 3 OS=Homo sapiens GN=RAC3 PE=1 SV=1	11	10	11	0	3	3	−1.90199	9.74646	0.00283	−1
sp|Q6UWD8|CP054_HUMAN Transmembrane protein C16orf54 OS=Homo sapiens GN=C16orf54 PE=1 SV=1	0	3	0	0	3	10	2.48165	8.53778	0.00343	1
sp|Q7Z403|TMC6_HUMAN Transmembrane channel-like protein 6 OS=Homo sapiens GN=TMC6 PE=1 SV=2	4	6	7	0	0	1	−3.36136	8.67516	0.00343	−1
sp|P22626|ROA2_HUMAN Heterogeneous nuclear ribonucleoproteins A2/B1 OS=Homo sapiens GN=HNRNPA2B1 PE=1 SV=2	13	7	18	37	13	8	1.08093	11.13039	0.00349	1
sp|P19338|NUCL_HUMAN Nucleolin OS=Homo sapiens GN=NCL PE=1 SV=3	17	18	20	11	5	0	−1.29355	10.64210	0.00351	−1
sp|P60174|TPIS_HUMAN Triosephosphate isomerase OS=Homo sapiens GN=TPI1 PE=1 SV=3	28	27	32	14	8	8	−1.05416	11.36084	0.00358	−1
sp|P21589|5NTD_HUMAN 5′-nucleotidase OS=Homo sapiens GN=NT5E PE=1 SV=1	5	0	0	8	9	0	2.17827	8.98862	0.00430	1

edgeR Analysis for Variably Expressed Proteins in the Cell Line Derived Vesicles

	MM1S Vesicle Spectral Count			U266 Vesicle Spectral Count			Statistics			
Identification	**Replicate 1**	**Replicate 2**	**Replicate 3**	**Replicate 1**	**Replicate 2**	**Replicate 3**	**logFC**	**logCPM**	**PValue**	**BH.mt.adj**
sp|P04406|G3P_HUMAN Glyceraldehyde-3-phosphate dehydrogenase OS=Homo sapiens GN=GAPDH PE=1 SV=3	114	106	133	58	46	49	−0.72866	13.46387	0.00439	−1
sp|P22234|PUR6_HUMAN Multifunctional protein ADE2 OS=Homo sapiens GN=PAICS PE=1 SV=3	5	14	5	4	0	0	−2.05215	9.31134	0.00440	−1
sp|O14818|PSA7_HUMAN Proteasome subunit alpha type-7 OS=Homo sapiens GN=PSMA7 PE=1 SV=1	5	2	3	0	0	0	−5.14456	7.82972	0.00467	−1
sp|Q13509|TBB3_HUMAN Tubulin beta-3 chain OS=Homo sapiens GN=TUBB3 PE=1 SV=2	48	42	33	21	15	11	−0.90824	11.89459	0.00473	−1
sp|P29966|MARCS_HUMAN Myristoylated alanine-rich C-kinase substrate OS=Homo sapiens GN=MARCKS PE=1 SV=4	24	18	27	33	31	27	0.87320	11.87273	0.00512	1
sp|P35241|RADI_HUMAN Radixin OS=Homo sapiens GN=RDX PE=1 SV=1	46	72	81	55	77	99	0.69101	13.31780	0.00544	1
sp|Q9HB71|CYBP_HUMAN Calcyclin-binding protein OS=Homo sapiens GN=CACYBP PE=1 SV=2	12	6	10	2	4	0	−1.71120	9.58566	0.00628	−1
sp|P26038|MOES_HUMAN Moesin OS=Homo sapiens GN=MSN PE=1 SV=3	128	198	208	175	201	210	0.61048	14.69934	0.00666	1
sp|P50990|TCPQ_HUMAN T-complex protein 1 subunit theta OS=Homo sapiens GN=CCT8 PE=1 SV=4	0	0	1	3	7	0	3.46006	7.98648	0.00794	1
sp|P05362|ICAM1_HUMAN Intercellular adhesion molecule 1 OS=Homo sapiens GN=ICAM1 PE=1 SV=2	20	12	25	18	27	29	0.84998	11.58227	0.00894	1
sp|P17612|KAPCA_HUMAN cAMP-dependent protein kinase catalytic subunit alpha OS=Homo sapiens GN=PRKACA PE=1 SV=2	6	3	0	0	0	0	−4.99708	7.67825	0.00898	−1
sp|P31943|HNRH1_HUMAN Heterogeneous nuclear ribonucleoprotein H OS=Homo sapiens GN=HNRNPH1 PE=1 SV=4	0	0	0	6	1	0	5.10776	7.33455	0.00898	1
sp|O94832|MYO1D_HUMAN Unconventional myosin-Id OS=Homo sapiens GN=MYO1D PE=1 SV=2	3	1	5	0	0	0	−4.99708	7.67923	0.00898	−1
sp|P10599|THIO_HUMAN Thioredoxin OS=Homo sapiens GN=TXN PE=1 SV=3	19	15	16	1	6	8	−1.24868	10.51947	0.01001	−1
sp|P27824|CALX_HUMAN Calnexin OS=Homo sapiens GN=CANX PE=1 SV=2	11	0	0	19	4	0	1.51621	9.61876	0.01125	1
sp|P09211|GSTP1_HUMAN Glutathione S-transferase P OS=Homo sapiens GN=GSTP1 PE=1 SV=2	47	50	45	28	17	14	−0.78826	12.13962	0.01157	−1
sp|P31146|COR1A_HUMAN Coronin-1A OS=Homo sapiens GN=CORO1A PE=1 SV=4	17	30	26	28	26	36	0.77633	11.90438	0.01191	1

edgeR Analysis for Variably Expressed Proteins in the Cell Line Derived Vesicles

	MM1S Vesicle Spectral Count			U266 Vesicle Spectral Count			Statistics			
Identification	**Replicate 1**	**Replicate 2**	**Replicate 3**	**Replicate 1**	**Replicate 2**	**Replicate 3**	**logFC**	**logCPM**	**PValue**	**BH.mt.adj**
sp|P04439|1A03_HUMAN HLA class I histocompatibility antigen; A-3 alpha chain OS=Homo sapiens GN=HLA-A PE=1 SV=2	43	37	37	41	46	49	0.69242	12.53684	0.01227	1
sp|P11233|RALA_HUMAN Ras-related protein Ral-A OS=Homo sapiens GN=RALA PE=1 SV=1	7	2	1	6	9	6	1.52000	9.48694	0.01230	1
sp|P51149|RAB7A_HUMAN Ras-related protein Rab-7a OS=Homo sapiens GN=RAB7A PE=1 SV=1	10	8	11	14	21	9	1.07058	10.72745	0.01245	1
sp|P61158|ARP3_HUMAN Actin-related protein 3 OS=Homo sapiens GN=ACTR3 PE=1 SV=3	16	14	13	3	6	4	−1.23585	10.30514	0.01368	−1
sp|P60953|CDC42_HUMAN Cell division control protein 42 homolog OS=Homo sapiens GN=CDC42 PE=1 SV=2	20	13	17	2	10	5	−1.07044	10.56161	0.01490	−1
sp|Q13813|SPTN1_HUMAN Spectrin alpha chain; non-erythrocytic 1 OS=Homo sapiens GN=SPTAN1 PE=1 SV=3	12	16	13	4	3	5	−1.28118	10.22922	0.01525	−1
sp|P20073|ANXA7_HUMAN Annexin A7 OS=Homo sapiens GN=ANXA7 PE=1 SV=3	3	1	2	10	4	2	1.84215	8.99118	0.01553	1
sp|P07948|LYN_HUMAN Tyrosine-protein kinase Lyn OS=Homo sapiens GN=LYN PE=1 SV=3	3	0	1	1	10	2	2.09886	8.61412	0.01672	1
sp|Q99828|CIB1_HUMAN Calcium and integrin-binding protein 1 OS=Homo sapiens GN=CIB1 PE=1 SV=4	5	8	3	0	0	2	−2.40587	8.67775	0.01672	−1